Chinese Chemical Letters 32 (2021) 2782–2786

Contents lists available at ScienceDirect

Chinese Chemical Letters

journal homepage: www.elsevier.com/locate/cclet

Communication

Isotypic heterojunction based on Fe-doped and terephthalaldehyde-modified carbon nitride for improving photocatalytic degradation with simultaneous hydrogen production

Xun-Heng Jiang[a,b,c,1], Fan Yu[b,c,1], Dai-She Wu[a], Lei Tian[a,b,c], Ling-Ling Zheng[a,b,c], Li-Sha Chen[a], Peng Chen[a,b,c], Long-Shuai Zhang[b,c,*], Hui Zeng[a,b,c], Ying Chen[a,b,c], Jian-Ping Zou[a,b,c,*]

[a] Key Laboratory of Poyang Lake Environment and Resource Utilization of Ministry of Education, School of Resources Environmental and Chemical Engineering, Nanchang University, Nanchang 330031, China
[b] Key Laboratory of Jiangxi Province for Persistent Pollutants Control and Resources Recycle, Nanchang Hangkong University, Nanchang 330063, China
[c] National-Local Joint Engineering Research Center of Heavy Metals Pollutants Control and Resource Utilization, Nanchang Hangkong University, Nanchang 330063, China

ARTICLE INFO

Article history:
Received 2 November 2020
Received in revised form 2 December 2020
Accepted 7 January 2021
Available online 12 January 2021

Keywords:
Isotypic heterojunction
Photocatalytic degradation
Simultaneous hydrogen evolution
Carbon nitride

ABSTRACT

To achieve an efficient photocatalytic for clean energy production and environmental remediation, the highly active Fe-doped and terephthalaldehyde-modified carbon nitride (Fe-CN/NTE) isotypic heterojunction photocatalyst is constructed *via* a simple annealing method for degradation of organic pollutants with simultaneous resource recovery. The Fe-CN/NTE catalyst exhibits a 93% removal rate of *p*-nitrophenol (4-NP) and a 1.72 mmol/g H_2 evolution rate in 2 h simultaneously under visible light irradiation, which are higher than those of pristine CN, Fe-CN, and NTE, respectively. Photoelectrochemical tests show that the excellent photocatalytic performance of Fe-CN/NTE comes from the improved migration, transportation, and separation of photoinduced charge carriers and expanded light-harvesting range. Moreover, hydroxyl radical ($^{\cdot}OH$), electron (e^-), and hole (h^+) are the main active species and the rational mechanism of 4-NP photodegradation was proposed based on scavenger measurements and liquid chromatography-mass spectrometry (LC–MS), respectively. Isotypic heterojunction Fe-CN/NTE photocatalyst possesses excellent stability in the H_2 evolution and 4-NP degradation during five-run cycle tests, posing as a promising candidate in practical works for organic pollution and energy challenges.

To date, environmental pollution and the energy crisis have become two major challenges [1–3]. Especially, water pollution caused by aromatics, hormones, and pesticides has attracted extensive attention since they are hardly degraded and possess high-toxicity [4–6]. Photocatalytic technology was considered a promising method to simultaneously tackle the above two issues because it consists of photocatalytic oxidation and reduction reactions [7–9]. Studies found that some organic pollutants can be degraded by photogenerated holes (h^+) or free radicals (hydroxyl radicals and superoxide anions) generated from solar energy conversion over photocatalysts, while CO_2 reduction or H_2 evolution from water splitting can be achieved using photogenerated electrons (e^-) [10–13]. However, if photocatalytic degradation of organic pollutants with simultaneous H_2 evolution would be fulfilled in a photocatalytic system, and the photocatalyst should possess suitable potentials of valance band (VB) and conduction band (CB) [14–16]. Therefore, it is urgent to develop photocatalytic systems suitable for simultaneous photocatalytic degradation of organic pollutants and H_2 evolution.

Graphitic carbon nitride (CN) has attracted extensive attention because of simple synthesis methods, widespread precursors, well visible light absorption, and metal-free [17–20]. However, the traditional thermal-induce polymerization of N-containing

* Corresponding authors at: Key Laboratory of Jiangxi Province for Persistent Pollutants Control and Resources Recycle, Nanchang Hangkong University, Nanchang 330063, China.
E-mail addresses: L_S_Zhang1990@163.com (L.-S. Zhang), zjp_112@126.com (J.-P. Zou).
[1] These authors contributed equally to this work.

https://doi.org/10.1016/j.cclet.2021.01.011

precursors typically formed a melon-based structure, which shows the relatively low photocatalytic efficiency due to a high recombination probability of photoexcited charge carriers [21–23]. To resolve these shortcomings, various strategies such as metal (Li, Na, and Fe) [24–26] or non-metallic (B, S, and P) [27–29] doping, organic co-monomers grafting [30,31], heterogeneous structures constructing [32–34], which could extend light absorption range, accelerate photogenerated charge migration and reduce charge recombination. Nevertheless, the extraneous materials usually exhibit clear differences between CN in physicochemical properties, which would greatly influence the compatibility, homogeneity, and stability of the resultant heterojunctions and also weaken the inherent advantages of CN [35–38]. Therefore, it is appealing to develop a CN-based isotypic heterojunction for the degradation of organic pollutants with simultaneous H_2 production.

Fe-doped CN had been proven to be an attractive method for eliminating high poisonous and stubborn organic pollution due to the adjustment of band structure and further enhance the light absorption of CN [39–41]. Also, terephthalaldehyde-modified CN was studied to vastly enhance photocatalytic H_2 evolution from water-splitting could be assigned to well boost photogenerated e^- transmission and higher charge separation, and reduced recombination of photogenerated electrons-holes into a π-conjugated polymeric network of CN [42]. To make these advantages, we are inspired to construct Fe-doped CN/terephthalaldehyde-modified CN composite with enhanced photocatalytic degradation and simultaneous H_2 production by integrating the functions of Fe doping and terephthalaldehyde modifying.

Herein, a new isotypic heterostructured photocatalyst consisted of Fe-doped CN (Fe-CN) and terephthalaldehyde-modified CN (Fe-CN/NTE) was prepared to fulfill photodegradation of *p*-nitrophenol (4-NP) with simultaneous photocatalytic H_2 generation. Furthermore, the relationship between photocatalytic degradation of 4-NP and the photocatalytic H_2 production was systematically investigated over these photocatalysts. As a result, the as-synthesized Fe-CN/NTE isotypic heterojunctions show superior photocatalytic degradation of 4-NP and simultaneous photocatalytic activity of H_2 evolution, and higher stability under visible light irradiation than that of pristine Fe-CN and NTE. Overall, this work not only elaborates on the synergistic photocatalytic mechanism which the effects of 4-NP and the rate of photocatalytic H_2 production, but also provides a new approach to achieve the goal of effective treatment of organic pollutants with simultaneous H_2 production.

The crystal construct of as-prepared catalysts was analyzed by XRD. As presented in Fig. 1a, there are two characteristic peaks located at around 12.9° and 27.6° of Fe-CN and NTE, corresponding to (100) and (002) planes, respectively, which indicates that the aldehydes grafting and Fe doping had no obvious effect on the texture of CN. However, the (002) peak of Fe-CN has a slight left shift compare to CN (Fig. 1b), disclosing that Fe doping can increase the layer spacing of CN, which was possibly originated from Fe locates between the adjacent layers of CN. Thus, the Fe atoms serve as an effective channel and accelerate charge transfer between layers.

As shown in (Figs. 1c and d), the as-synthesized catalysts exhibit the characteristic FTIR vibrations peaks of CN at 810, 1244, 1324, 1458, and 1632 cm^{-1}, which is assigning to the skeletal vibrations of tri-s-triazine ring (C_6N_7) units of CN. And the peak at 1410 cm^{-1} associated with the stretching vibrations of the s-triazine ring (C_3N_3) units. Compare with CN, a weak characteristic peak of the C=C at 1506 cm^{-1} can be observed in the FTIR spectrum of NTE, demonstrating that aromatic rings were successfully grafted onto the CN networks. Expectantly, the FTIR spectrum of Fe-CN/NTE shows two characteristic peaks at 1506 and 1365 cm^{-1}, which are attributed to aromatic ring carbon and s-triazine stretching vibration, respectively. Based on these results, the isotypic heterojunction Fe-CN/NTE have been fabricated successfully.

The chemical structure of the as-synthesized catalysts was further investigated by NMR and XPS. As shown in Fig. 2a, the ^{13}C spectra of the CN and NTE show two resonance peaks at δ_1 = 164.9 ppm and δ_2 = 156.7 ppm, which can be ascribed to the C atoms in CN_2 and CN_3 groups in C_3N_3, respectively. Besides, the chemical shift at 131.6 ppm is assigned to phenyl carbons in the NTE, indicating the benzene rings successfully modified CN. The remaining peak at 162.9 ppm can be assigned to amine carbon to link C_3N_3 and benzene rings. These results confirm terephthalaldehyde was successfully grafted on the CN. The XPS C 1s spectra of CN, NTE, Fe-CN, and Fe-CN/NTE (Fig. 2b) reveals three peaks centered at 284.6, 285.2, and 288.2 eV, which are assigned to C—C/C=C, C—N—H_x, and N—C=N in the C_3N_3, respectively. In

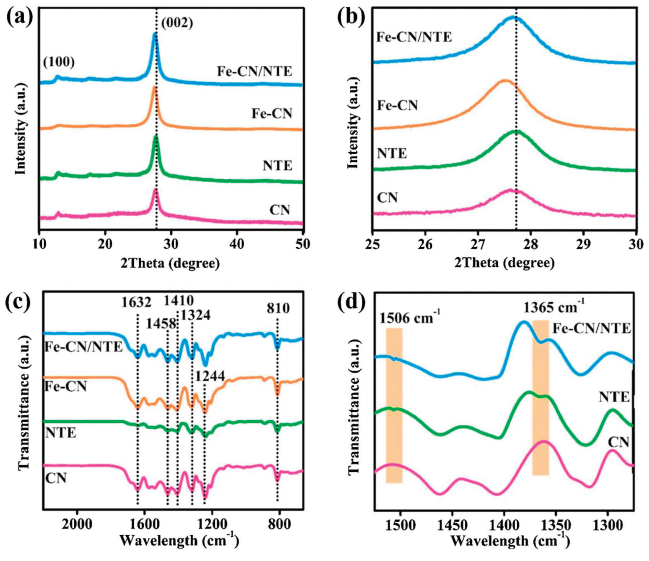

Fig. 1. (a) XRD patterns of the as-prepared CN, NTE, Fe-CN, and Fe-CN/NTE, and (b) enlarged profile of the (002) peak. (c) FTIR spectra of the as-prepared CN, NTE, Fe-CN, and Fe-CN/NTE and (d) enlarged profile of FTIR spectra in the range of 1260–1540 cm^{-1} of the as-prepared CN, NTE, and Fe-CN/NTE.

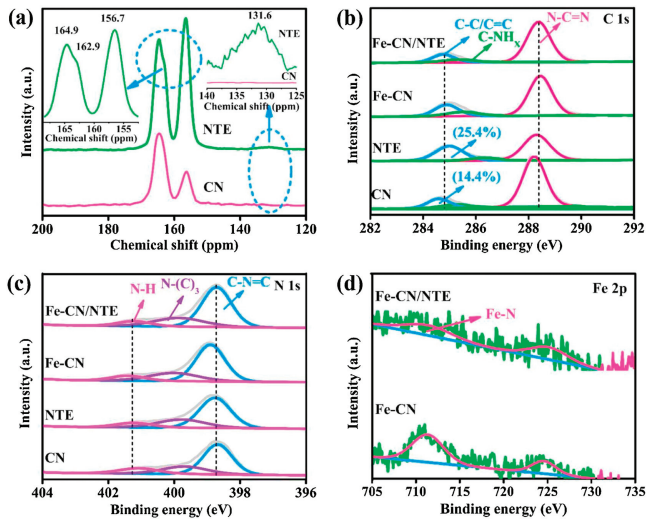

Fig. 2. (a) Solid-state MAS-^{13}C NMR spectra of the CN and NTE. (b) XPS for C 1s spectrum and (c) N 1s spectrum of the CN, NTE, Fe-CN, and Fe-CN/NTE. (d) Fe 2p high-resolution XPS spectra of the Fe-CN and Fe-CN/NTE.

comparison with CN, the peak intensity of NTE at 284.9 eV increases from 14.4% to 25.4%, suggesting that aromatic rings have been successfully introduced into the framework of CN, which is also supported by the FTIR analysis. Besides, the N 1s spectrum of CN is also confirmed by three peaks at 398.7, 399.7, and 401.1 eV, which are identified as C–N=C, N–$(C)_3$, and N–H_x groups in the heptazine framework, respectively. And these peaks of C 1s and N 1s spectra for Fe-CN shift to higher binding energy than CN, which is attributed to the chemical state of hybridized aromatic N changed after Fe doping. Since the lone-pair electrons in the nitrogen pots of CN occupied the free orbital of the central Fe form Fe–N moieties, resulting in lower electron density as well as the higher binding energy of N atom (Fig. 2c). And the N 1s featured peaks originated from amino function (C—N—H) of the hetero-structure Fe-CN/NTE is located between NTE and Fe-CN in Fig. 2c, indicating a strong chemical interaction between the two components. Moreover, the valent state of the central Fe was also described in Fig. 2d, two obvious peaks of Fe-CN at 724.2 and 711.4 eV belong to Fe $2p_{1/2}$ and Fe $2p_{3/2}$, respectively. The binding energy of Fe $2p_{3/2}$ is higher than that of Fe-CN, demonstrating that Fe(III) was successfully coordinated with the N atom to form Fe(III)–N moieties [43]. These aforesaid results have confirmed the existence of NTE and Fe-CN in the Fe-CN/NTE isotypic hetero-junction.

As depicted in Fig. 3a, the Fe-CN/NTE shows better visible light absorption compared with the CN, NTE, and Fe-CN. And the photocurrent intensities of the as-prepared samples (Fig. 3b) show the order of CN < Fe-CN < NTE < Fe-CN/NTE, indicating that the Fe-CN/NTE possesses the best efficiency in term of separation rate of photo-generated e^- and h^+ among the as-synthesized samples. Fig. 3c displays photoluminescence (PL) spectra of the CN, NTE, Fe-CN, and Fe-CN/NTE samples measured at an excitation wavelength of 315 nm. Among these catalysts, the Fe-CN and NTE exhibit a lower PL intensity than that of CN, indicating that Fe doping and terephthalaldehyde grafting are favorable for inhibiting the recombination of photogenerated e^- and h^+. Expectantly, the intensity of Fe-CN/NTE becomes weaker after the successfully composite of Fe-CN and NTE, which reveals that the isotypic heterojunction Fe-CN/NTE presents the most separation efficient of photogenerated e^- and h^+. Electrochemical impedance spectra were recorded to investigate the electrochemical properties of the samples. As shown in Fig. 3d, the Fe-CN/NTE shows the smallest resistance among the as-prepared catalysts, indicating that the best efficient charge separation occurred in the Fe-CN/NTE. And Fig. S2 (Supporting information) depicts a clear dividing line between Fe-CN and NTE. The above results confirm that the formation of Fe-CN/NTE can effectively promote light absorption and separation of photo-generated e^- and h^+, and further improve the photocatalytic performance.

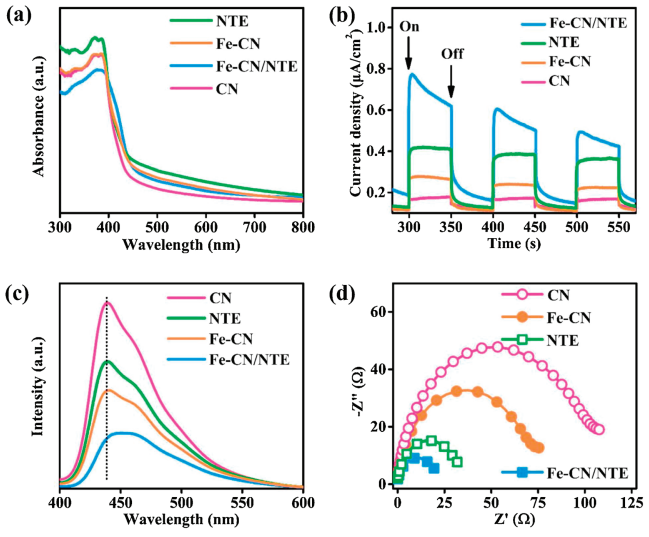

Fig. 3. (a) UV–vis absorption spectra, (b) transient photocurrent spectra, (c) PL spectra, and (d) electrochemical impedance spectra of the as-prepared catalysts.

To enhance photocatalytic activities with an H_2 evolution and photocatalytic degradation of the organic pollutants over the CN, we try to combine NTE with Fe-CN to construct the heterojunction of Fe-CN/NTE. And as shown in Fig. S3 (Supporting information), the 30%Fe-CN/NTE shows the highest photocatalytic activities. Additionally, the photocatalytic performance of degradation of 4-NP combine with H_2 evolution under visible light irradiation over the as-prepared catalysts was shown in Fig. 4a. The CN expresses only photocatalytic activity with an H_2 evolution rate of 0.179 mmol g^{-1} h^{-1} and 4-NP removal rate of 3.2% after 2 h photocatalytic reaction. Moreover, the Fe-CN and NTE showed higher photodegradation rate of 4-NP and H_2 evolution rate than that of CN, indicating that Fe doping achieves a better visible light response, and terephthalaldehyde modifying get desired electronic structures into the π-conjugated polymeric network of CN, and extend the delocalization of π electrons to change the intrinsic properties. Benefiting from these advantages, the Fe-CN/NTE shows the highest photocatalytic activities with a 93% removal rate of 4-NP and H_2 evolution rate of 0.86 mmol g^{-1} h^{-1} in 2 h. Besides, the influence of different initial concentrations of 4-NP was also studied. As shown in Fig. 4b, the H_2 evolution rate and the removal rate of 4-NP also enhances as a gradual increase of initial concentration of 4-NP, implying that more 4-NP molecules could be absorbed on the surface of the Fe-CN/NTE at a higher initial concentration of 4-NP, which is beneficial for photocatalytic degradation along with more used by the derived intermediates give rise to a lower photocatalytic H_2 evolution rate. As shown in Fig. 4c, the H_2 evolution rate slightly increased with prolonged reaction time are attributed to both catalyst activation and platinum deposition take a certain time of Fe-CN/NTE, whereas the photocatalytic removal rate of 4-NP only had a little decrease after five cycles, suggesting that the Fe-CN/NTE can be efficiently recycled.

The active radical species during a photocatalytic reaction, such as $^{\bullet}OH$, e^-, and h^+ were detected by *tert*-butyl alcohol (*t*-BuOH),

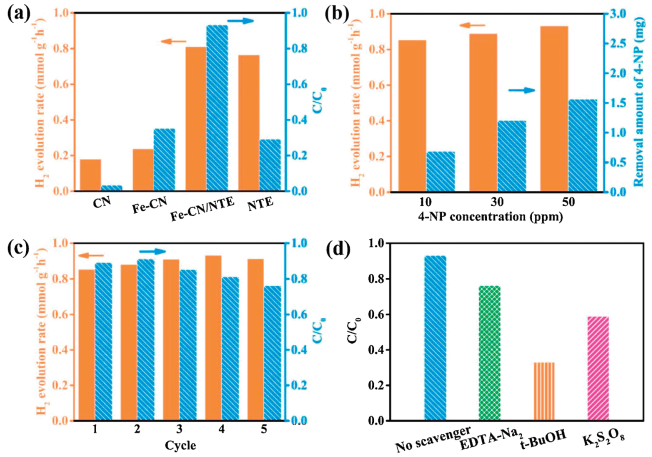

Fig. 4. (a) The combination of degradation of 4-NP with hydrogen evolution under visible light irradiation over the as-prepared catalysts. (b) Simultaneous photo-degradation of organic pollutants coupled with hydrogen evolution by using the 30%Fe-CN/NTE at a different initial concentration of 4-NP. (c) Cycling test in the closed gas system over the 30%Fe-CN/NTE under visible light. (d) The removal efficiency of 4-NP over the Fe-CN/NTE after the addition of different scavengers for a 2 h reaction.

potassium persulfate ($K_2S_2O_8$), and ethylenediaminetetraacetic acid (EDTA-Na_2), respectively. As shown in Fig. 4d, the photocatalytic degradation efficiency of 4-NP was significantly inhibited when the *t*-BuOH and EDTA-Na_2 were added, indicating that the $^{\bullet}OH$ and h^+ are the main active species in the photocatalytic degradation of the 4-NP process. Moreover, the TA-PL technique was used to confirm the amount of $^{\bullet}OH$ radicals during photocatalysis [44,45]. The maximum absorption peak (Fig. S4 in Supporting information) is gradually strengthening along with increase the irradiation time, suggesting that the Fe-CN/NTE catalyst produces $^{\bullet}OH$ during a photocatalytic reaction. Besides, the photodegradation efficiency of 4-NP was also obviously restrained with adding $K_2S_2O_8$, which- implied that photogenerated e^- also had a promoting effect on the degradation of 4-NP in agreement with the experimental results of effect on the different initial concentration of 4-NP on H_2 production. Namely, in part of photogenerated e^- are used to produce $^{\bullet}OH$ for photodegradation of 4-NP, whereas remaining photogenerated e^- are utilized for hydrogen production.

Besides, to further elucidate the photocatalytic mechanism, the generated intermediates and final products during the photodegradation of 4-NP were detected by LC–MS. As shown in Fig. S5 (Supporting information), the characteristic signal peak of 4-NP can be assigned to the MS fragmentation pattern at *m/z* 138. During the process of photocatalytic degradation of 4-NP, the characteristic pattern at *m/z* 138 had significantly decreased, and some intermediates at *m/z* 74, 96, 104, 108, 116, 128, and 144 were observed. The results indicate that the degradation mechanism of 4-NP is hydroxylation and demethylation reactions. Then, these intermediates were further mineralized by $^{\bullet}OH$ or e^- to form CO_2 and H_2O. According to the above analyses, the possible degradation pathways of 4-NP was proposed in Fig. 5. For the first path, the hydroxyl group (–OH) favors the electrophilic attack of $^{\bullet}OH$ on the ortho and para-positions connecting with a crack of hydrogen bondings in the benzene ring. Afterward, it generated hydroquinone or catechol, which were determined by the characteristic patterns at *m/z* 108 and 110, respectively. Furthermore, the $^{\bullet}OH$ radicals attack the aromatic ring to generate some intermediates (*m/z* 72, 76 104, 118, and 144) and are ultimately mineralized to CO_2 and H_2O. For the second path of 4-NP degradation, a successive electrophilic attack of $^{\bullet}OH$ on hydroquinone forms hydroxyquinol (*m/z* 128), which would be transformed into 5-hydroxycyclohex-2-ene-1,4-dione (*m/z* 116) after accepting e^-. Afterward, the intermediates ring-open to generate some carboxylic acids (fumaric acid and oxalic acids confirmed by the characteristic patterns at *m/z* 116 and 104), and eventually are mineralized to CO_2 and H_2O *via* $^{\bullet}OH$. The above results confirm that e^- the competition would occur between the 4-NP photodegradation and photocatalytic production of H_2. Therefore, the photogenerated e^- are not all acted on photocatalytic H_2 production, resulting in a decrease of photocatalytic efficiency of H_2 production.

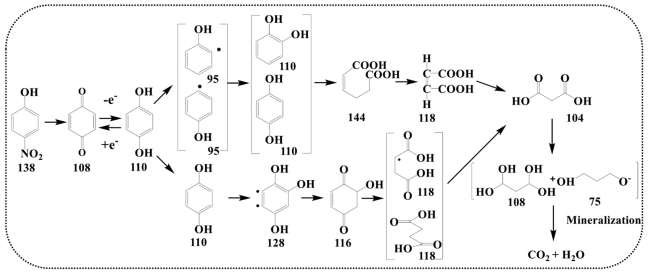

Fig. 5. Proposed degradation mechanisms of 4-NP by the Fe-CN/NTE photocatalyst under visible light irradiation.

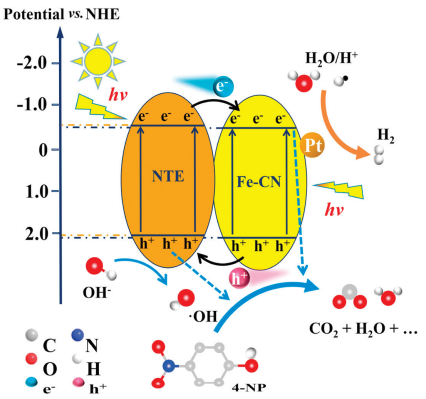

Scheme 1. Possible photocatalytic mechanism of degradation of 4-NP coupled with simultaneous photocatalytic H_2 evolution over the Fe-CN/NTE under visible light irradiation.

According to the Mott–Schottky plots of NTE and Fe-CN, the CB potentials of NTE and Fe-CN are obtained as −0.56 and −0.41 V *vs.* NHE, respectively (Fig. S6 in Supporting information). Combined with the optical bandgap of NTE and Fe-CN, the VB potentials of NTE and Fe-CN are calculated as 2.17 V and 2.27 V, respectively, which are more positive than that of $^{\bullet}OH/OH^-$ (1.99 V *vs.* NHE). Hence, h^+ on the VB of NTE can react with OH^- in solution to obtain $^{\bullet}OH$. Also, the oxidation potentials of 4-NP are 0.94 V [15,16], which is smaller than the VBs of the NTE and Fe-CN. Thus, 4-NP can be directly oxidized by the photogenerated h^+ on the VB of NTE, which is consistent with the above results of the scavenger test and photocatalytic performance experiment. As shown in Scheme 1, when the Fe-CN/NTE catalyst was illuminated under visible light radiation, Fe-CN and NTE can absorb light to generate e^- and h^+. Then, the e^- on the CB of NTE transfers to the CB of Fe-CN, and further react with water molecular or hydrogen proton on the surface of photo deposited Pt to form H_2. For the photodegradation of 4-NP, a small amount of e^- will be used for the degradation of intermediates of 4-NP, therefore the photocatalytic rate of H_2 evolution over Fe-CN/NTE in the 4-NP solution is lower than that in the pure water solution. Hence, the h^+ on the VB of NTE transfers to the VB of Fe-CN, and then gradually decompose 4-NP to CO_2 and H_2O. Moreover, 4-NP can also be mineralized by $^{\bullet}OH$ generated from OH^- oxidation *via* h^+.

In this work, Fe-CN/NTE composite catalysts have been successfully designed and prepared by combining Fe-CN and NTE *via* a simple annealing method. Systematic characterizations were done to successfully verify the Fe-CN/NTE heterostructured composite. Among the as-prepared catalysts, the Fe-CN/NTE catalyst exhibits the best efficiency of 4-NP degradation rate under visible light irradiation and synergistically photocatalytic H_2 evolution rate from water splitting, which are mainly attributed to the perfectly enhance light-harvesting, and improve separation of photoinduced charge carriers. Also, the present work systematically clarifies the concentration effect of 4-NP on the photocatalytic rate of H_2 evolution, then 4-NP and their intermediate products are also mineralized *via* h^+, e^-, and $^{\bullet}OH$. A reasonable mechanism was presented to explain the enhancement of photocatalytic degradation 4-NP and simultaneous H_2 evolution over the Fe-CN/NTE catalyst.

Declaration of competing interest

The authors report no declarations of interest.

Acknowledgments

We gratefully acknowledge the financial support of the National Natural Science Foundation of China (Nos. 51868050, 51938007, and 51878325), the Natural Science Foundation of Jiangxi Province (Nos. 20171ACB20017, 20171BAB206049, and 20202BAB213011), the Key Research and Development Project of Jiangxi Province (No. 20181BBG78034) and the Scientific Research Foundation of Nanchang Hangkong University (No. EA201902377).

Appendix A. Supplementary data

Supplementary material related to this article can be found, in the online version, at doi:https://doi.org/10.1016/j.cclet.2021.01.011.

References

[1] H.R. Wei, S.K. Loeb, J.H. Kim, et al., Proc. Natl. Acad. Sci. 117 (2020) 15473–15481.
[2] T. Takata, J.Z. Jiang, K. Domen, et al., Nature 581 (2020) 411–414.
[3] F. Chen, H.W. Huang, Y.H. Zhang, et al., Chin. Chem. Lett. 28 (2017) 2244–2250.
[4] Y. Yang, G.M. Zeng, D.L. Huang, et al., Water Res. 184 (2020) 116200.
[5] Y.B. Chen, J.F. Li, Z.Q. Liu, et al., Chin. Chem. Lett. 31 (2020) 1516–1519.
[6] L. Tian, H.L. Jiang, X.B. Luo, et al., Chem. Eng. J. 343 (2018) 607–618.
[7] D.D. Zheng, X.N. Cao, X.C. Wang, Angew. Chem. Int. Ed. 55 (2016) 11512–11516.
[8] C.C. Dong, M.Y. Xing, J.L. Zhang, et al., Environ. Sci. Technol. 52 (2018) 11297–11308.
[9] Y.G. Zhou, X.X. Wang, G.H. Yu, et al., Proc. Natl. Acad. Sci. 116 (2019) 10232–10237.
[10] Y.C. Zhang, N. Afzal, J.J. Zou, et al., Adv. Sci. 6 (2019) 1900053.
[11] L. Pan, J.J. Zou, W.B. Mi, et al., Nat. Commun. 11 (2020) 418.
[12] N. Chen, H. Li, L.Z. Zhang, et al., Environ. Sci. Technol. 52 (2018) 12656–12666.
[13] X.H. Jiang, L.S. Zhang, J.P. Zou, et al., Angew. Chem. Int. Ed. 59 (2020) 23112–23116.
[14] A. Kumar, A. Rana, F.J. Stadler, et al., ACS Appl. Mater. Interfaces 10 (2018) 40474–40490.
[15] Y.C. Nie, J.P. Zou, S.L. Suib, et al., App. Catal. B: Environ. 227 (2018) 312–321.
[16] X.H. Jiang, Q.J. Xing, J.P. Zou, et al., ACS Sustainable Chem. Eng. 6 (2018) 12695–12705.
[17] S.V.P. Vattikuti, P.A.K. Reddy, C. Byon, et al., ACS Omega 3 (2018) 7587–7602.
[18] W.J. Ong, L.L. Tan, S.P. Chai, et al., Chem. Rev. 116 (2016) 7159–7329.
[19] G.F. Liao, H.Y. Gao, G.J. Yang, et al., Energy Environ. Sci. 12 (2019) 2080–2147.
[20] L.H. Lin, X. Cai, X.C. Wang, et al., Nat. Catal. 3 (2020) 649–655.
[21] F. Yu, F.R. Ai, J.P. Zou, et al., Chin. Chem. Lett. 31 (2020) 1648–1653.
[22] L.S. Zhang, D.M. Li, Q.B. Meng, et al., Adv. Funct. Mater. 29 (2019) 1806774.
[23] Y. Zheng, Y.L. Chen, X.C. Wang, et al., Adv. Funct. Mater. 30 (2020) 2002021.
[24] L.W. Ruan, G.S. Xu, Y.J. Zhu, et al., Mater. Res. Bull. 66 (2015) 156–162.
[25] L.S. Zhang, D.M. Li, Q.B. Meng, et al., Nano Res. 11 (2018) 2295–2309.
[26] G.M. Liu, G.H. Dong, Y.B. Zeng, et al., Chin. J. Catal. 41 (2020) 1564–1572.
[27] Y.T. Wang, T. Yang, J.H. Wang, et al., Nanoscale 10 (2018) 4913–4920.
[28] H.J. Kong, D.H. Won, S.I. Woo, et al., Chem. Mater. 28 (2016) 1318–1324.
[29] J.R. Ran, T.Y. Ma, S.Z. Qiao, et al., Energy Environ. Sci. 8 (2015) 3708–3717.
[30] W. Che, Q.H. Liu, S.Q. Wei, et al., J. Am. Chem. Soc. 139 (2017) 3021–3026.
[31] Y. Yu, W.G. Song, K.J. Ding, et al., J. Mater. Chem. A 5 (2017) 17199–17203.
[32] P.Y. Kuang, L. Zhuo, Z.Q. Liu, et al., Appl. Sur. Sci. 358 (2015) 296–303.
[33] J.H. Liu, L.M. Duan, Y.G. Zhang, et al., Nano Lett. 16 (2016) 6568–6575.
[34] K. Wei, K.X. Li, S.L. Luo, et al., App. Catal. B: Environ. 222 (2018) 88–98.
[35] Q.H. Liang, Z.H. Huang, Q.H. Yang, et al., Small 13 (2017) 1603182.
[36] Z.G. Liu, G. Wang, P. Yang, et al., Chem. Commun. 54 (2018) 4720–4723.
[37] L.B. Jiang, X.Z. Yuan, J. Liang, et al., Environ. Sci. Nano 5 (2018) 2604–2617.
[38] Z.Y. Fang, Y.J. Bai, W.D. Shi, et al., Nano Energy 75 (2020) 104865.
[39] J.S. Hu, Y.H. Liang, W.Q. Cui, et al., App. Catal. B: Environ. 245 (2019) 130–142.
[40] S. Mandal, S.Y. Pu, X.K. Wang, et al., Sci. Total Environ. 708 (2020) 134831.
[41] Y. Huang, J. Zhang, W.K. Ho, et al., Solar RRL 4 (2020) 202000170.
[42] J.J. Tian, L.X. Zhang, J.L. Shi, et al., J. Mater. Chem. A 4 (2016) 13814–13821.
[43] H.C. Li, C. Shan, B.C. Pan, Environ. Sci. Technol. 52 (2018) 2197–2205.
[44] X.H. Jiang, J.P. Zou, X.K. Wang, et al., App. Catal. B: Environ. 228 (2018) 29–38.
[45] Q.Y. Yi, J.L. Zhang, M.Y. Xing, et al., Environ. Sci. Technol. 53 (2019) 9725–9733.